DOI: 10.1002/anie.200801369

Imaging Probe

A Hybrid Nanoparticle Probe for Dual-Modality Positron Emission Tomography and Magnetic Resonance Imaging**

Jin-sil Choi, Jeong Chan Park, Hyunsoo Nah, Seungtae Woo, Jieun Oh, Kyeong Min Kim, Gi Jeong Cheon, Yongmin Chang, Jeongsoo Yoo, and Jinwoo Cheon**

As the accurate imaging of biological targets becomes an increasingly important tool for understanding basic biological phenomena and for fault-free diagnosis of various diseases,[1] current single-modality imaging methods tend to be inadequate. Therefore, multimodal imaging can be an essential tool in state-of-the-art imaging research and also standard practice in the clinic.[2] By combining dual- and triple-modality methods, many shortcomings that are present for single-modality imaging methods can be overcome. For example, the simultaneous use of positron emission tomography (PET), for its highly sensitive functional imaging, and computed tomography (CT), for its ability to provide clear anatomical information, has been demonstrated for the early detection of cancer.[2b] Several combinations of imaging methods with different modalities, such as magnetic resonance (MR)/optical[2c] and PET/near-infrared optical fluorescence (NIRF),[2d] are possible. Recently, the development of a dual-modality diagnostic instrument for PET/MR imaging (MRI) has been demonstrated.[2e]

[*] J. C. Park,[+] J. Oh, Prof. J. Yoo
Department of Molecular Medicine and Nuclear Medicine
CMRI, Kyungpook National University, Daegu 700-422 (Korea)
Fax: (+82) 53-426-4944
E-mail: yooj@knu.ac.kr
J.-s. Choi,[+] H. Nah, Prof. J. Cheon
Department of Chemistry, Yonsei University
Seoul 120-749 (Korea)
Fax: (+82) 2-364-7050
E-mail: jcheon@yonsei.ac.kr
S. Woo
Department of Biomedical Engineering
Kyungpook National University, Daegu 700-422 (Korea)
Prof. Y. Chang
Department of Molecular Medicine and Diagnostic Radiology
Kyungpook National University, Daegu 700-422 (Korea)
Dr. K. M. Kim, Dr. G. J. Cheon
Molecular Imaging Research Center
Korea Institute of Radiological and Medical Sciences
Seoul 139-706 (Korea)
[+] These authors contributed equally to this work.

[**] This work was partially supported by the KRF (MOEHRD, Basic Research Promotion Fund) (KRF-2007-331-E00166), KOSEF (R15-2004-033-06001-0), NRL (R0A-2006-000-10255), AOARD (FA4869-07-1-4016), Nano/Bio Program (M10503000218-05M0300-21810), the Korea Research Council of Fundamental Science & Technology, NCI Center for Cancer Nanotechnology Excellence, and the BK21 program of chemistry and medical college. Production of ^{124}I was supported partially by the QURI project of MOST and KOSEF.
Supporting information for this article is available on the WWW under http://dx.doi.org/10.1002/anie.200801369.

In addition to the instrumental advances of the diagnostic hardware, the development of nanoparticle-based probes is a prerequisite for successful multimodal diagnostics.[3] Quantum dots have been labeled with radioisotopes or paramagnetic metal ions to serve as NIRF-based dual-modality probes.[3a–g] Superparamagnetic iron oxide (SPIO) nanoparticles have been labeled with fluorescent dyes for MR/optical dual-modality imaging.[3h,i] The SPIO nanoparticle conjugated with ^{64}Cu and fluorescent dye as a new class of trimodal probe was demonstrated for macrophage detection in atherosclerotic plaques by using PET/CT imaging in comparison to MRI.[3j]

Herein, we report a magnetic-nanoparticle-based PET/MRI probe and the evaluation of its effectiveness as an in vivo dual-modality imaging agent. Noninvasive imaging and three-dimensional tomography are important advantages of PET and MRI.[1] In Figure 1, the imaging characteristics of MR and

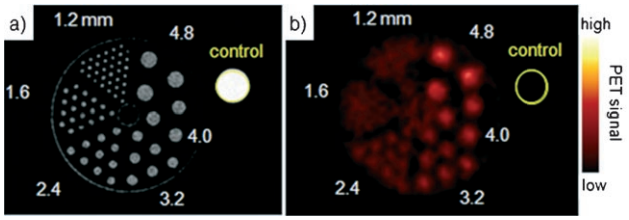

Figure 1. Comparison of spatial resolution of a) MRI and b) PET techniques with a Derenzo phantom (circle diameters of 1.2, 1.6, 2.4, 3.2, 4.0, and 4.8 mm), which contains the contrast agents MnMEIO (50 $\mu g\,mL^{-1}$ (Mn + Fe)) and ^{124}I (2.5 $\mu Ci\,mL^{-1}$); yellow circle: water (control). MnMEIO = Mn-doped magnetism-engineered iron oxide.

PET are compared by using a Derenzo phantom filled with a solution of contrast agents. In the MR image, all circles ranging from 1.2 to 4.8 mm in diameter are well resolved (Figure 1a) and it is possible to go further down to a resolution of 250 μm (see the Supporting Information, Figure S1). On the other hand, the PET image shows relatively poor spatial resolution and only circles larger than 2.4 mm in diameter are resolved (Figure 1b).

Although the MR probe provides better spatial resolution, in terms of sensitivity the PET probe shows an enhanced contrast effect, with picogram-scale sensitivity compared to the microgram-scale sensitivity of the MR probe (see below).[1a] Therefore, combining the merits of the individual imaging techniques through a single hybrid probe would make PET/MR dual modality an ideal candidate for a variety of biological studies. We chose the sentinel lymph node (SLN) as a model biological subject. The lymphatic system is an

important first line of defense against infection, and it is also used as a route for the metastasis of malignant cancer.[4] Hence, accurate localization and characterization of SLNs is critical for cancer staging.[4c–f]

We first prepared MnMEIO with a composition of $MnFe_2O_4$, which has an exceptionally high MR contrast effect.[5] Its measured *T*2 relaxivity coefficient (r_2) of 321.6 $mM^{-1}s^{-1}$ is two or three times better than that of conventional iron oxide-based SPIO probes[6] (see the Supporting Information, Figure S2). The MnMEIO nanoparticle surface was exchanged with serum albumin (SA) to ensure high colloidal stability in a wide pH range and at high salt concentration. The carboxylic and amine groups of SAs are cross-linked by using *N*-(3-dimethylaminopropyl)-*N*-ethylcarbodiimide hydrochloride and *N*-hydroxysulfosuccinimide to further stabilize the SA coatings. These SA-MnMEIO nanoparticles possess excellent nanoprobe characteristics with a monodispersed core size of 15 nm (Figure 2a) and a hydrodynamic size of 32 nm including the SA coating (Figure 2b). This probe size of 32 nm is especially critical, because lymphatic imaging agents for SLN mapping should meet a size criterion of 5–40 nm for the hydrodynamic diameter. Otherwise the probe cannot be confined in the lymphatic ducts or its mobility within the lymphatic track will be limited.[7] SA-MnMEIO probes are stable in up to 1M salt solutions and at pH values between 1 and 11 (Figure 2c).

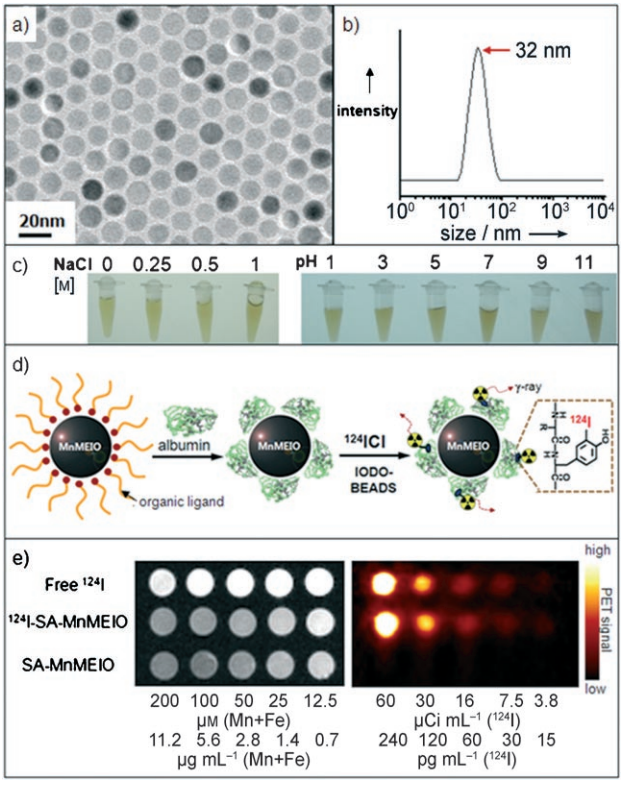

Figure 2. a) Transmission electron microscopy image of 15-nm MnMEIO. Synthesized MnMEIO is highly monodispersed ($\sigma < 5\%$). b) Hydrodynamic size of SA-MnMEIO in aqueous solution. c) Stability of SA-MnMEIO in aqueous solution at different salt concentrations and pH values. d) Preparation of ^{124}I-SA-MnMEIO. e) MR (left) and PET images (right) of free ^{124}I, ^{124}I-SA-MnMEIO, and SA-MnMEIO at various concentrations. ^{124}I-SA-MnMEIO clearly exhibits the dual characteristics of PET and MRI.

Because ^{124}I, a PET radionuclide, can be directly conjugated to the tyrosine residue in SA, SA-MnMEIO is an efficient platform for the formation of PET/MR hybrid nanoprobes (Figure 2d). SA-MnMEIO was conjugated with ^{124}I ($t_{1/2} = 4.2$ days, β^+ 23%) by using Iodo-Beads (Pierce Biochemical Co., USA).[8] Iodo-Beads with iodide ion in solution result in oxidation and the subsequent formation of a reactive mixed-halogen species, ^{124}ICl, which reacts with the *ortho* position of tyrosine (Figure 2d).

To evaluate any possible interference between the two imaging modalities of superparamagnetic nanoparticles and radioactive iodide ions when combined into a single hybrid probe, the MRI and PET data of ^{124}I-labeled SA-MnMEIO (^{124}I-SA-MnMEIO) were compared with those of SA-MnMEIO and free ^{124}I ions. Across the various concentrations of nanoparticle probes, ^{124}I-SA-MnMEIO did indeed maintain equivalent contrast effects corresponding to the probe of each imaging modality (Figure 2e).

We utilized ^{124}I-SA-MnMEIO dual-modality probes for the imaging of two different lymph nodes (LNs).[9] Imaging of SLNs is difficult, especially when located deep inside tissue, but very important for understanding cancer metastasis because cancer cells migrate through them. Upon injection of ^{124}I-SA-MnMEIO nanoprobes (229 μg kg^{-1} (Mn + Fe); ^{124}I activity: 110 μCi) into the right forepaw of a rat, the anatomical upper body shape is clearly obtained in addition to a few dark spots in the coronal view of the MR image taken 1 h post injection (Figure 3a,h). In the PET image, the upper strong red spot is from the forepaw injection site and the lower one is from the brachial LNs (white circle, Figure 3b).

Although PET is a highly sensitive imaging technique, it does not provide any anatomical information. The accurate positioning of a brachial LN (white circle, Figure 3c) in the context of the anatomical shape of a rat is only clearly achieved when the PET and MR images are overlaid. To confirm the above imaging results, the brachial LNs from both the right- and left-hand sides were dissected and reexamined by PET and MRI. Consistent with in vivo imaging results, only the LN on the right-hand side exhibited strong PET and MR signals relative to the contra-lateral brachial LN (Figure 3g).

Imaging of the other, axillary LN is challenging because it is further away from the injection site and positioned deeper than the brachial LN, which is the first SLN encountered.[9] The beauty of our dual PET/MR probes is seen in the transverse images (Figure 3d–f), in which two different LNs can be clearly identified. In the MR images, a brachial LN is observed as a strong dark spot in the lower right-hand side (white circle, Figure 3d), but unambiguous assignment of a faint dark spot as an axillary LN is difficult (red circle, Figure 3d). As a complementary technique, the observation of two spots in the PET image is critical (Figure 3e,i). When images from the two modalities are overlaid, a blue spot in the PET image clearly matches with the MRI-detected position and confirms it as an axillary LN, while the stronger red/blue spot coincides with the MRI-determined position that originated from the brachial LN (Figure 3f). Note that the very low background in the PET images indicates that the ^{124}I-SA-

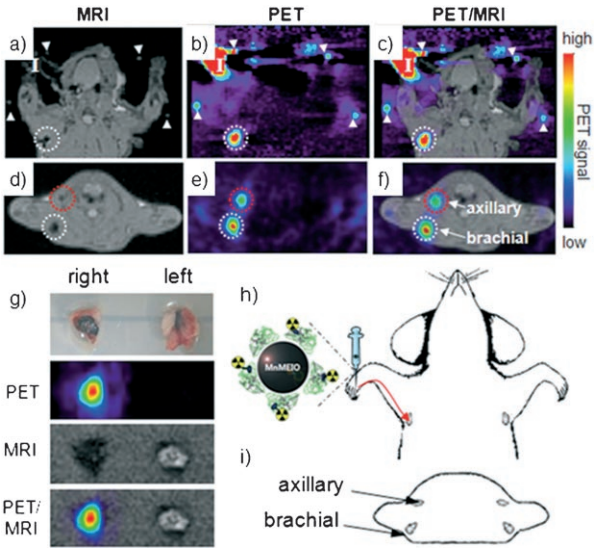

Figure 3. a–f) PET/MR images of SLNs in a rat at 1 h post injection of ^{124}I-SA-MnMEIO into the right forepaw (I = nanoprobe injection site). Coronal a) MR and b) PET images in which a brachial LN (white circle) is detected. c) The position of the brachial LN is well matched in a PET/MR fusion image. Four small pipette tips containing Na^{124}I solution are used as a fiducial marker (white arrowheads) for the concordant alignment in PET/MR images. In the transverse images, axillary (red circle) and brachial LNs (white circle) are detected in the d) MR and e) PET images, and images of each node are nicely overlapped in the corresponding PET/MR fusion image (f). g) The explanted brachial LN also shows consistent results with in vivo images by PET and MR. Only the LN from the right-hand side of the rat containing ^{124}I-SA-MnMEIO shows strong PET and dark MR images. The schematics of the rat in the h) coronal and i) transverse directions show the locations of the LNs.

MnMEIO dual probes are highly stable under physiological conditions; ^{124}I did not become detached from the ^{124}I-SA-MnMEIO probes and the intact ^{124}I-SA-MnMEIO moved along the lymphatic duct. In long-term six-day follow-up studies by MRI, the uptake of ^{124}I-SA-MnMEIO in LNs peaked at one day, and afterward the probe was gradually cleared out (see the Supporting Information, Figure S5).

In conclusion, we have successfully developed a nanoparticle-based probe for dual-modality PET/MRI, in which two different types of LNs could be clearly identified and accurately localized in a PET/MR fusion image as a result of the highly complementary nature of the PET and MRI techniques. In addition to diagnostics, the detected SLNs could be further monitored in real time by using a hand-held gamma probe to allow precise surgical operation.[10] As the size of biomedical probes is often critical for their efficient delivery to targeted areas, such as cancer cells and LNs, another advantage of the dual-modality probes lies in the simplified total control of the size of the probes that results from the precise tunability of inorganic nanoparticles. Such hybrid-type probes would be useful for noninvasive and highly sensitive real-time imaging of various biological events, including cell migration, cancer diagnosis, and drug delivery.

Experimental Section

Preparation of cross-linked SA-MnMEIO: SA-MnMEIO nanoparticles (2 mg) were dispersed in phosphate-buffered saline (1 mL, 0.01 mol, pH 7.2), and *N*-(3-dimethylaminopropyl)-*N*-ethylcarbodiimide hydrochloride (9.6 mg, 50 μmol) and *N*-hydroxysulfosuccinimide (1.2 mg, 5 μmol) were added to the solution. The reaction was carried out for 2 h at room temperature. Cross-linked SA-MnMEIO was purified with a desalting column (GE Healthcare, USA).

Derenzo phantom imaging: The circles of the Derenzo phantom (1.2, 1.6, 2.4, 3.2, 4.0, and 4.8 mm in diameter) were filled with an aqueous solution containing SA-MnMEIO (50 μg mL^{-1} (Mn + Fe)) and [^{124}I]NaI (2.5 μCi mL^{-1}). The MR image was obtained by a *T*2-weighted fast gradient-echo sequence at 1.5 T (repetition time (TR) = 8.0 ms, echo time (TE) = 3.2 ms, matrix = 256 × 256, field of view (FOV) = 10 × 10 cm, slice thickness = 0.8 mm). The PET image was obtained with a Concorde PET R4 Rodent Model scanner (Concorde Microsystems Inc., Knoxville, TN). Data were collected for 6 h in a detector energy window of 460–580 keV. Two-dimensional reconstruction of the image was performed by an ordered-subsets expectation maximization (OSEM) algorithm.

Measurement of r_2 of SA-MnMEIO: The SA-MnMEIO solution was prepared at concentrations of 0.1, 1, 10, and 100 μg mL^{-1} (Mn + Fe). The *T*2 relaxivity coefficient r_2 was measured by using different echo times in a fast spin-echo sequence (TR = 4000, TE = 10, 30, 60, 90, 120, 150, 180, 210, 240, 270, 300, 350, 400, 450, 500, 550, 600, 650, 700, 750, 800, 850, 900, 950, 1400, 1500, 1800, and 1900 ms, FOV = 9 × 9 cm, matrix = 320 × 160, slice thickness = 5 mm).

Labeling of SA-MnMEIO with ^{124}I: SA-MnMEIO (80 μg (Mn + Fe)) and ^{124}I (1 mCi, $t_{1/2}$ = 4.2 days, β^+ 23 %) were mixed with activated Iodo-Beads and reacted for 15 min. The labeling yield was determined by radio-TLC. The ^{124}I-SA-MnMEIO was purified from unlabeled free ^{124}I by centrifugation (Microcon YM-50, Amicon, USA). The radiochemical purity after purification was higher than 92 %.

PET and MRI: Reconstituted ^{124}I-SA-MnMEIO (80 μg, 110 μCi) in saline (< 70 μL) was injected subcutaneously into the right front paw of Sprague–Dawley rats (male, 12 weeks old). Small-animal dedicated PET (R4 Rodent Model, Concorde Microsystems Inc., USA) was used to obtain dynamic PET images for 1 h. During PET and MRI, rats were anesthetized by inhalation of a mixture of isoflurane and oxygen. Immediately after the PET scan, MRI was performed by a 3D fast gradient-echo sequence at 1.5 T (TR = 8.0 ms, TE = 3.2 ms, flip angle = 20°, bandwidth = 31.25 kHz, FOV = 10 × 10 cm, locs per slab = 34, matrix = 256 × 256, number of experiments = 8). For reproducible positioning and precise co-registration of PET/MR images, animal-specific molds were fabricated by using fiber clay. Four small pipette tips containing [^{124}I]NaI solution were inserted around rats as a fiducial marker. Fusion of PET and MRI was performed manually by using four fiducial markers in the AMIDE program.

Resection of LNs: After PET and MR images were obtained, brachial LNs on both sides were resected at 40 min post injection of methylene blue dye. Resected LNs were fixed on 1 % agarose gel. PET and MR images were taken under the previous conditions.

Received: March 21, 2008
Revised: May 14, 2008
Published online: July 9, 2008

Keywords: imaging agents · magnetic resonance imaging · manganese · nanoparticles · positron emission tomography

[1] a) T. F. Massoud, S. S. Gambhir, *Gene. Dev.* **2003**, *17*, 545; b) K. Shah, A. Jacobs, X. O. Breakefield, R. Weissleder, *Gene Ther.*

2004, *11*, 1175; c) L. Ottobrini, P. Ciana, A. Biserni, G. Lucignani, A. Maggi, *Mol. Cell. Endocrinol.* **2006**, *246*, 69.
[2] a) S. R. Cherry, *Annu. Rev. Biomed. Eng.* **2006**, *8*, 35; b) A. D. Jorn, V. V. Wouter, H. M. Corstens Frans, J. G. Oyen Wim, *Cancer Imaging* **2007**, *7*, 77; c) P. M. Marites, Y. Wang, X. Wen, A. B. James, L. C. Stephens, S. Jasser, G. G. Juri, N. M. Jeffrey, C. Li, *Invest. Radiol.* **2007**, *42*, 569; d) L. Sampath, S. Kwon, S. Ke, W. Wang, R. Schiff, E. M. Michel, M. S.-M. Eva, *J. Nucl. Med.* **2007**, *48*, 1501; e) M. S. Judenhofer, H. F. Wehrl, D. F. Newport, C. Catana, S. B. Siegel, M. Becker, A. Thielscher, M. Kneilling, M. P. Lichy, M. Eichner, K. Klingel, G. Reischl, S. Widmaier, M. Röcken, R. E. Nutt, H.-J. Machulla, K. Uludag, S. R. Cherry, C. D. Claussen1, B. J. Pichler, *Nat. Med.* **2008**, *14*, 459.
[3] a) W. Cai, K. Chen, Z.-B. Li, S. Gambhir, X. Chen, *J. Nucl. Med.* **2007**, *48*, 1862; b) H. Yang, S. Santra, G. A. Walter, P. H. Holloway, *Adv. Mater.* **2006**, *18*, 2890; c) L. Prinzen, R. H. M. Miserus, A. Dirksen, T. M. Hackeng, N. Deckers, N. J. Bitsch, R. T. A. Megens, K. Douma, J. W. Heemskers, M. E. Kooi, P. M. Frederik, D. W. Slaaf, M. J. Van Zandvoort, C. P. M. Reutelingsperger, *Nano Lett.* **2007**, 7, 93; d) A. J. Lucas, R. C. Hawkes, R. E. Ansorge, G. B. Williams, R. E. Nutt, J. C. Clark, T. D. Fryer, T. A. Carpenter, *Technol. Cancer Res. Treat.* **2006**, *5*, 337; e) V. S. Talanov, C. A. S. Regino, H. Kobayashi, M. Bernardo, P. L. Choyke, M. W. Brechbiel, *Nano Lett.* **2006**, *6*, 1459; f) W. J. Mulder, R. Koole, R. J. Brandwijk, G. Storm, P. T. Chin, G. J. Strijkers, C. M. Donega, K. Nicolay, A. W. Griffioen, *Nano Lett.* **2006**, *6*, 1; g) O. Veiseh, C. Sun, J. Gunn, N. Kohler, P. Gabikian, D. Lee, N. Bhattarai, R. Ellenbogen, R. Sze, A. Hallahan, J. Olson, M. Zhang, *Nano Lett.* **2005**, *5*, 1003; h) L. Josephson, M. F. Kircher, U. Mahmood, Y. Tang, R. Weissleder, *Bioconjugate Chem.* **2002**, *13*, 554; i) J.-H. Lee, Y.-w. Jun, S.-I. Yeon, J.-S. Shin, J. Cheon, *Angew. Chem.* **2006**, *118*, 8340; *Angew. Chem. Int. Ed.* **2006**, *45*, 8160; j) M. Nahrendorf, H. Zhang, S. Hembrador, P. Panizzi, D. E. Sosnovik, E. Aikawa, P. Libby, F. K. Swirski, R. Weissleder, *Circulation* **2008**, *117*, 379.
[4] a) B. Misselwitz, *Eur. J. Radiol.* **2006**, *58*, 375; b) L. L. Muldoon, P. Varallyay, D. F. Kraemer, G. Kiwic, K. Pinkston, S. L. Walker-Rosenfeld, E. A. Neuwelt, *Neuropathol. Appl. Neurobiol.* **2004**, *30*, 70; c) A. Luciani, E. Itti, A. Rahmounia, M. Meignan, O. Clement, *Eur. J. Radiol.* **2006**, *58*, 338; d) P. Wunderbaldinger, *Eur. J. Radiol.* **2006**, *58*, 325; e) T. Barrett, P. L. Choyke, H. Kobayashi, *Contrast Media Mol. Imaging* **2006**, *1*, 230; f) A. M. Wallace, C. K. Hoh, S. J. Ellner, D. D. Darrah, G. Schulteis, D. R. Vera, *Ann. Surg. Oncol.* **2007**, *14*, 913.
[5] J.-H. Lee, Y.-M. Huh, Y.-w. Jun, J.-w. Seo, J.-t. Jang, H.-T. Song, S. Kim, E.-J. Cho, H.-G. Yoon, J.-S. Suh, J. Cheon, *Nat. Med.* **2007**, *13*, 95.
[6] Y.-X. J. Wang, S. M. Mussain, G. P. Krestin, *Eur. Radiol.* **2001**, *11*, 2319.
[7] J. M. Jeong, M. K. Hong, Y. J. Kim, J. Lee, J. H. Kang, D. S. Lee, J.-K. Chung, M. C. Lee, *Nucl. Med. Commun.* **2004**, *25*, 1211.
[8] M. A. K. Markwell, *Anal. Biochem.* **1982**, *125*, 427.
[9] a) W. Van den Broeck, A. Derore, P. Simoens, *J. Immunol. Methods* **2006**, *312*, 12; b) C. W. Jung, J. M. Rogers, E. V. Groman, *J. Magn. Magn. Mater.* **1999**, *194*, 210; c) J. M. Rogers, C. W. Jung, J. Lewis, E. V. Groman, *Magn. Reson. Imaging* **1998**, *16*, 917.
[10] S. Maza, M. Taupitz, K. Taymoorian, K. J. Winzer, J. Rückert, C. Paschen, G. Räber, S. Schneider, U. Trefzer, D. L. Munz1, *Eur. J. Nucl. Med. Mol. Imaging* **2007**, *34*, 378.

